JCB Journal of Cell Biology

ARTICLE

mRNP architecture in translating and stress conditions reveals an ordered pathway of mRNP compaction

Anthony Khong[1,2] and Roy Parker[1,2]

Stress granules (SGs) are transient membraneless organelles of nontranslating mRNA–protein complexes (mRNPs) that form during stress. In this study, we used multiple single-molecule FISH probes for particular mRNAs to examine their SG recruitment and spatial organization. Ribosome runoff is required for SG entry, as long open reading frame (ORF) mRNAs are delayed in SG accumulation, indicating that the SG transcriptome changes over time. Moreover, mRNAs are ∼20× compacted from an expected linear length when translating and compact ∼2-fold further in a stepwise manner beginning at the 5′ end during ribosome runoff. Surprisingly, the 5′ and 3′ ends of the examined mRNAs were separated when translating, but in nontranslating conditions the ends of long ORF mRNAs become close, suggesting that the closed-loop model of mRNPs preferentially forms on nontranslating mRNAs. Compaction of ribosome-free mRNAs is ATP independent, consistent with compaction occurring through RNA structure formation. These results suggest that translation inhibition triggers an mRNP reorganization that brings ends closer, which has implications for the regulation of mRNA stability and translation by 3′ UTR elements and the poly(A) tail.

Introduction

Stress granules (SGs) are transient membraneless organelles of nontranslating mRNA–protein complexes (mRNPs) that form when translation is limited (Buchan and Parker, 2009; Panas et al., 2016; Protter and Parker, 2016). SGs are important because they are a cellular marker for translation status and play a role in the stress response (Kedersha et al., 2013), and because mutations that inhibit SG disassembly or clearance are implicated in several degenerative diseases such as amyotrophic lateral sclerosis and multisystem proteinopathy (Dewey et al., 2012; Buchan et al., 2013; Kim et al., 2013; Li et al., 2013; Ramaswami et al., 2013; Mackenzie et al., 2017). Moreover, the study of SGs may provide new insights into the assembly, organization, and functions of other non–membrane-bound RNA bodies such as the nucleolus, Cajal bodies, paraspeckles, and processing bodies.

SGs are enriched for mRNAs that are long and poorly translated (Khong et al., 2017; Namkoong et al., 2018). This suggests a model wherein long mRNPs that exit translation during stress form numerous interactions with other long nontranslating mRNPs, leading to the formation of SGs. Some of these interactions that facilitate SG formation are mediated by RNA-binding proteins (Protter and Parker, 2016), but intermolecular RNA–RNA interactions also appear to contribute to SG formation and to defining the SG transcriptome (Van Treeck et al., 2018). An unresolved issue is the relative timing of mRNPs exiting translation in response to stress and accumulating in SGs.

The timing of SG formation and the enrichment of long mRNAs in SGs creates a conundrum. SGs form within the first 10–15 min after the addition of arsenite (Kedersha et al., 2000; Wheeler et al., 2016), yet mRNAs with long ORFs, such as the SG-enriched mRNA AHNAK and DYNC1H1, which both have ORFs >10 kb long (Khong et al., 2017), require at least 15 min for ribosome runoff once translation initiation is blocked. One possibility is that these long mRNAs can accumulate in SGs once a portion of their ORF is exposed and devoid of ribosomes, even if ribosomes near the 3′ end of the ORF are still elongating. Another possibility is that elongating ribosomes are removed from these mRNAs without having to reach the termination codon, perhaps by a mechanism analogous to ribosome quality control (Harigaya and Parker, 2010; Shoemaker et al., 2010; Brandman et al., 2012; Shoemaker and Green, 2012; Chiabudini et al., 2014; Brandman and Hegde, 2016). Finally, it is also possible that mRNAs with a long ORF are slower at getting to SGs, which would require the SG transcriptome to change over time.

[1]Howard Hughes Medical Institute, University of Colorado, Boulder, CO; [2]Department of Biochemistry, University of Colorado, Boulder, CO.

Correspondence to Roy Parker: roy.parker@colorado.edu.

We used multiple smFISH probes for specific mRNAs to examine the timing of mRNA entry to SGs as well as their overall mRNP architecture, which revealed key aspects of mRNA targeting to SGs. First, complete ribosome runoff is required for mRNAs to enter SGs, as mRNAs with long ORFs are delayed in SG accumulation. This demonstrates that the SG transcriptome changes over time. We also observed that mRNAs are compacted from their expected linear length when translating, and compact even further in a stepwise manner because of ribosome runoff. We do not see evidence for the closed-loop model of mRNP organization while mRNAs are engaged in translation, although the distance between the 5′ and 3′ ends of long mRNAs shrinks disproportionally compared with the rest of the mRNA body when mRNAs become untranslated. We suggest the possibility that the closed-loop structure of mRNPs preferentially forms on nontranslating mRNPs.

Results

mRNAs with long ORFs are recruited to SGs more slowly than mRNAs with shorter ORFs

To determine the relationship between SG assembly and the recruitment of mRNAs with long ORFs, we measured the extent of SG localization of several SG-enriched mRNAs (Khong et al., 2017) with various ORF lengths in U-2 OS cells (Nancy Kedersha and Paul Anderson, Brigham and Women's Hospital, Boston, MA) treated with arsenite for 15, 30, 45, and 60 min by single-molecule FISH (smFISH). These include AHNAK, DYNC1H1, NORAD, PEG3, ZNF704, CDK6, and NORAD RNAs. AHNAK and DYNC1H1 mRNAs have long ORFs (~17.5 and 14 kb, respectively), whereas the PEG3 and ZNF704 mRNAs have shorter ORFs (~4.7 and 1.2 kb, respectively). The CDK6 mRNA is valuable because it has a short ORF (~1 kb) but a very long 3′ UTR (~10 kb), allowing us to distinguish effects of the overall transcript length from ORF length. We also examined when a long noncoding RNA, NORAD, is recruited to SGs. The predicted ribosome runoff times (estimated using a translation elongation speed of 18 ribonucleotides/second) for these mRNAs once translation initiation is blocked are shown in Table 1. We performed these experiments in U-2 OS cells where arsenite induces robust eIF2α phosphorylation, which can be used as an approximate marker for when translation initiation is inhibited. Previous analysis indicated that in U-2 OS cells, translation initiation is inhibited by ~8 min after arsenite addition (Wheeler et al., 2016).

A key result was that individual RNAs accumulated in SGs at different times, in a manner that correlated with their ORF length. Specifically, we observed that when cells were stressed for 30 min with arsenite, the long-ORF mRNAs, AHNAK and DYNC1H1 mRNAs, were minimally recruited to SGs (12%; Fig. 1, A and B; and Fig. S1). In contrast, RNAs with shorter ORFs (PEG3, ZNF704, and CDK6) or no ORFs (NORAD) were recruited to a greater degree (39–55%) at 30 min (Fig. 1, A and B; and Fig. S1). These results suggest the mRNA composition of SGs changes over time during arsenite stress, and although mRNAs with longer ORFs are highly enriched in SGs (Khong et al., 2017), they accumulate slower.

Two additional observations suggest that the difference in the timing of mRNA recruitment to SGs is caused by elongating ribosomes. First, treatment of U-2 OS cells with arsenite and puromycin, which releases all elongating ribosomes from mRNAs, causes the AHNAK and DYNC1H1 mRNAs to be recruited to SGs at earlier times (30 min, $P < 0.001$), whereas recruitment of NORAD, PEG3, ZNF704, and CDK6 RNAs showed no increase in recruitment at 30 min (not significant; Fig. 1, A and C; and Fig. S2). Second, treatment of U-2 OS cells with cycloheximide after 30 min of arsenite exposure, which traps elongating ribosomes on mRNAs, stops the accumulation of all RNAs in SGs (Fig. 1, A and D; and Fig. S3).

Table 1. **Ribosome runoff time**

mRNA	Total length (nt)	ORF length (nt)	Predicted ribosome runoff time (18 nt/s)
AHNAK	18,836	17,673	~16 min
DYNC1H1	14,361	13,941	~13 min
PEG3	8,765	4,767	~4 min
ZNF704	14,403	1,239	~1 min
CDK6	11,661	981	~1 min

AHNAK and DYNC1H1 mRNPs are generally compact under nonstress conditions

In other work, we had observed that during stress the 5′ and 3′ ends of the AHNAK mRNA were often close together (Moon et al., 2018 *Preprint*). Similar compaction of three other mRNAs under a variety of stress conditions has been observed (Adivarahan et al., 2018). To examine the overall architecture of mRNAs during normal and stress conditions, and how it related to mRNA entry into SGs, we used smFISH probes to the 5′ end, the 3′ end, and throughout the middle of the AHNAK and DYNC1H1 mRNAs (Figs. 2 A and 3 A). We first used these probes on unstressed cells where mRNAs are engaged in translation. We measured the distances between the center of the signal for each probe in three dimensions (see Materials and methods), which allowed us to determine the distribution of spacing for these probe sets on individual mRNA molecules.

We discovered that both AHNAK and DYNC1H1 mRNAs are more compact than expected from linear or hairpin models of translating mRNPs (Figs. 2 B and 3 B), with most distances between different segments of AHNAK mRNPs <300 nm (Fig. 2, B and C). The distances between the 5′ and 3′ ends of AHNAK mRNAs are usually larger (median ~200 nm) than the distances between the 5′ end and middle (median ~150 nm) or the 3′ end and middle of AHNAK mRNPs (median ~150 nm). These distance measurements are much shorter than expected from the AHNAK mRNA contour length (5.4 μm) or from a possible polysome hairpin, which would be ~2.7 μm. We estimate that the degree of compaction for the AHNAK mRNA relative to its contour length is ~27-fold (using the median distance between the 5′ and 3′ ends compared with the extended contour length) or 18-fold (using the median distance between one end and the middle relative to half the contour length). We obtained similar results for the DYNC1H1 mRNA with the median compaction relative to DYNC1H1 mRNA contour length estimated to

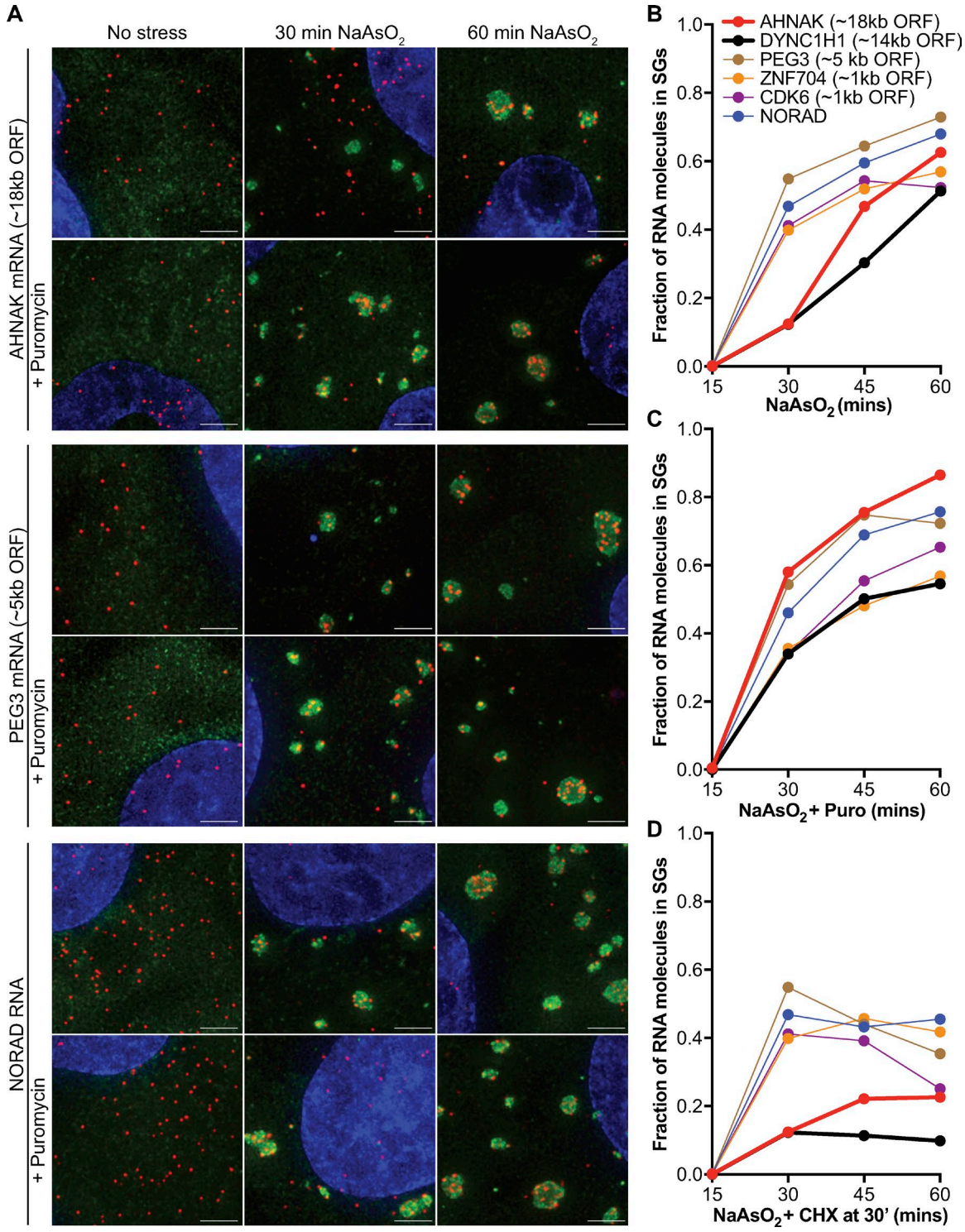

Figure 1. **mRNA recruitment to SGs is dependent on when ribosomes run off mRNAs after translation inhibition. (A)** Representative smFISH images acquired for three different transcripts (AHNAK, PEG3, and NORAD) for U-2 OS cells treated with 0.5 mM $NaAsO_2$ with or without 10 µg/ml puromycin for 30 or 60 min. Nuclei (blue), G3BP1 (green), and individual RNA (red). Scale bar: 2 µm. **(B–D)** Fraction of specific RNA molecules found in SGs at 15, 30, 45, and 60 min in U-2 OS when stressed with 0.5 mM $NaAsO_2$ (B), 0.5 mM $NaAsO_2$ (C), and 10 µg/ml puromycin, and 0.5 mM $NaAsO_2$ with 50 µg/ml cycloheximide (D) added after cells were stressed for 30'. More than 250 RNAs were counted for each sample. The 15 and 30 min results shown in D are identical to the 15- and 30-min result shown in B.

be between 21- and 14-fold (Fig. 3, B and C). Similar compaction values were also observed for three other long mRNAs in translating conditions by Adivarahan et al. (2018). These results show that long mRNAs are not in an extended conformation even when engaged in translation and suggest possible mechanisms of mRNA compaction (see Discussion).

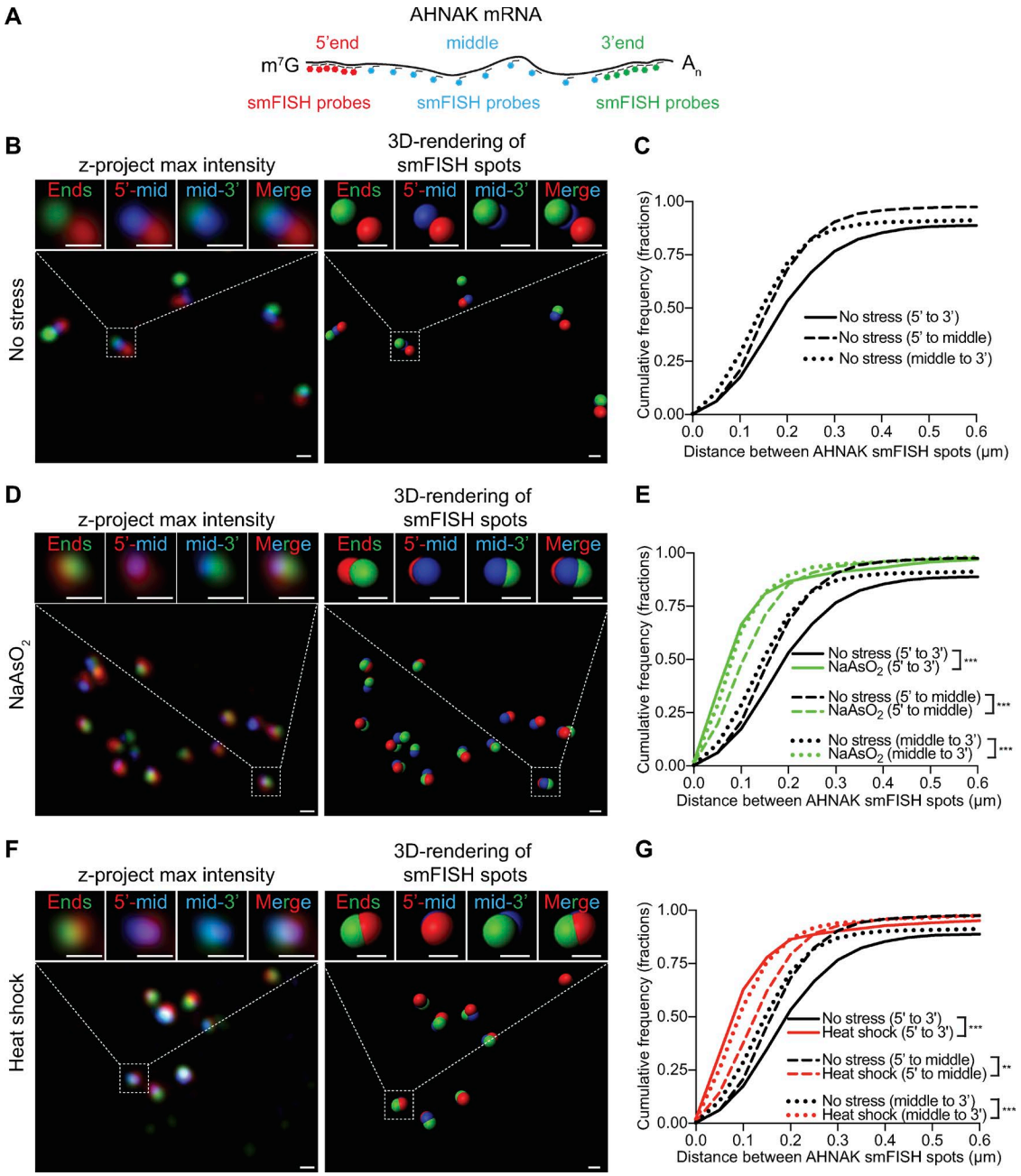

Figure 2. **Organization of AHNAK mRNPs in nonstress and stress conditions. (A)** Cartoon schematic indicating where smFISH probes bind to AHNAK mRNAs. smFISH probes binding to the 5′ ends, middle, or 3′ ends are labeled with distinct fluorophores and are false-colored red, blue, and green, respectively. **(B, D, and F)** Left: Representative AHNAK smFISH images of U-2 OS cells that were not stressed (B) or stressed with 0.5 mM $NaAsO_2$ for 60 min (D) or heat shock at 42°C for 60 min (F). Right: 3D rendering of smFISH spots by Bitplane Imaris imaging analysis software. Scale bar: 250 nm. **(C, E, and G)** Cumulative frequency graphs (in fractions) of smallest distances between 5′ to 3′ end smFISH spots (solid lines), 5′ end to middle smFISH spots (dash lines), and middle to 3′ end smFISH spots (dotted lines) in unstressed cells (black), 0.5 mM $NaAsO_2$-treated cells (green), and heat shock cells (red). More than 850 smallest distances were quantified for each sample (n = 1,189 [no stress], n = 1,062 [$NaAsO_2$], and n = 860 [heat shock]). The nonstress samples are identical in panels C, E, and G and in Fig. 4 B. **, P ≤ 0.01; ***, P ≤ 0.001 (Student's two-tailed t test).

AHNAK and DYNC1H1 mRNPs compact further under stress conditions

A similar analysis during stress conditions revealed that the distances between all three smFISH spots for AHNAK and DYNC1H1 mRNAs shrink considerably under arsenite-treated conditions (Fig. 2, D and E; and Fig. 3, D and E). For example, the median distance between the 5′ and 3′ ends, 5′ end and middle, and 3′ end and middle of AHNAK mRNAs are now ∼90, ∼130, and ∼100 nm, respectively. Relative to the contour length, the median compaction of AHNAK mRNAs in U-2 OS cells treated with arsenite is ∼62- or 24-fold: ∼62-fold if we measure the compaction by dividing the median end-to-end distances to the contour length and ∼24-fold if we measure the compaction by dividing the median end-to-middle distances to half

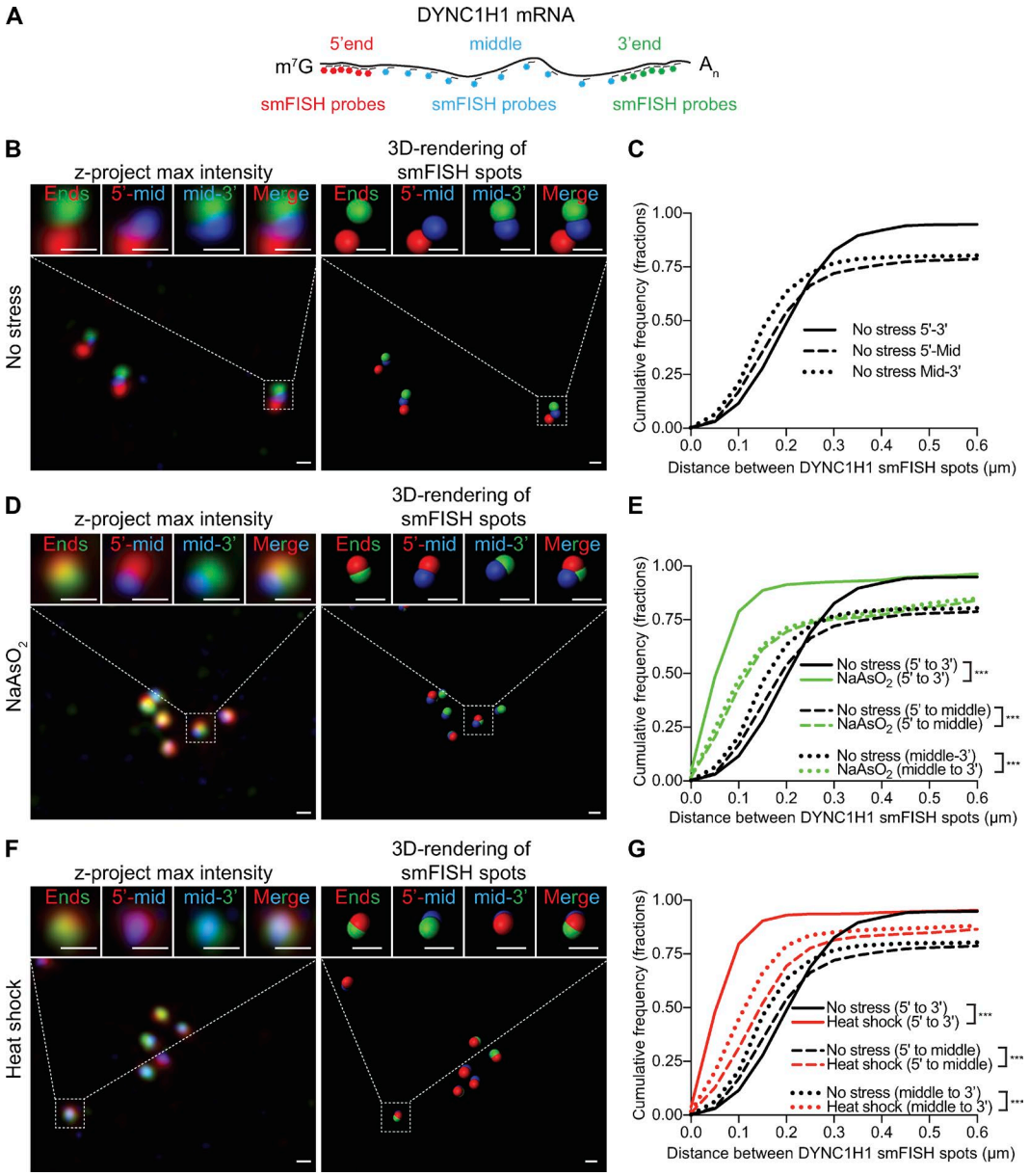

Figure 3. **Organization of DYNC1H1 mRNPs in nonstress and stress conditions. (A)** Cartoon schematic indicating where smFISH probes bind to DYNC1H1 mRNAs. smFISH probes binding to the 5′ ends, middle, or 3′ ends are labeled with distinct fluorophores and are false-colored red, blue, and green, respectively. **(B, D, and F)** Left: Representative DYNC1H1 smFISH images of U-2 OS cells that were not stressed (B) or stressed with 0.5 mM $NaAsO_2$ for 60 min (D) or heat shock at 42°C for 60 min (F). Right: 3D rendering of smFISH spots by Bitplane Imaris imaging analysis software. Scale bar: 250 nm. **(C, E, and G)** Cumulative frequency graphs (in fractions) of smallest distances between 5′ to 3′ end smFISH spots (solid lines), 5′ end to middle smFISH spots (dash lines), and middle to 3′ end smFISH spots (dotted lines) in unstressed cells (black), 0.5 mM $NaAsO_2$-treated cells (green), and heat shock cells (red). More than 1,000 smallest distances were quantified for each sample (n = 1,113 [no stress], n = 1,032 [$NaAsO_2$], and n = 1,056 [heat shock]). The no stress samples are identical in panels C, E, and G and in Fig. 4 D. The smallest distances between the 5′ and middle and the 3′ and middle smFISH spots reach a cumulative frequency of ∼75% within 600 nm because the middle smFISH probes are not as effective and for ∼25% of DYNC1H1 mRNAs, a middle smFISH spot was not detected. ***, P ≤ 0.001 (Student's two-tailed t test).

the contour length. Similar compaction values were also seen with DYNC1H1 mRNAs (Fig. 3, D and E). The distances between all three smFISH spots for AHNAK and DYNC1H1 mRNAs also shrink considerably in heat shock conditions compared with nonstressed U-2 OS cells, with similar compaction values (Fig. 2, F and G; and Fig. 3, F and G). Thus, in multiple stresses that inhibit translation initiation, we and others (Adivarahan et al., 2018) observe enhanced mRNP compaction.

Increased compaction of AHNAK and DYNC1H1 mRNPs under stress is a consequence of ribosome release from mRNA

Because 80% of AHNAK and 53% of DYNC1H1 mRNAs are found in arsenite-induced SGs at 60 min, and similar percentages were seen for heat shock-induced SGs at 60 min (Khong et al., 2017), we expect the compaction measurements for AHNAK and DYNC1H1 mRNAs are reflective of AHNAK and DYNC1H1 mRNAs found inside SGs. Because of technical limitations, we

have not been able to examine all three smFISH probes simultaneously with an SG marker. However, smFISH staining indicates that most AHNAK and DYNC1H1 mRNAs tend to cluster during stress, as expected by their strong enrichment in SG (Fig. 2, D and F; and Fig. 3, D and F). This suggests that most AHNAK and DYNC1H1 mRNPs form compact assemblies inside SGs during a stress response.

In principle, the increased compaction of AHNAK and DYNC1H1 mRNPs in SGs might be a consequence of ribosome release from mRNA and/or a consequence of increased macromolecular crowding possibly occurring inside SGs compared with the cytosol. We performed three analyses to distinguish these possibilities. First, we measured the distances between the 5′ and 3′ ends of AHNAK and DYNC1H1 mRNPs inside and outside SGs (Fig. 4 H). We observed that the distances between the 5′ and 3′ ends of AHNAK and DYNC1H1 mRNPs showed a similar distribution inside and outside SGs (Fig. 4 H), consistent with the increased compaction being independent of SG accumulation.

In a second experiment, we examined the organization of AHNAK and DYNC1H1 mRNPs by smFISH when U-2 OS cells were treated with puromycin (Fig. 4, A–D). Addition of puromycin leads to release of elongating ribosomes (Pestka, 1971) but does not lead to SG assembly, perhaps because translation initiation is ongoing and even partial ribosome engagement appears to block mRNA accumulation in SG (see Discussion). We observed that puromycin is sufficient to lead to increased compaction of the AHNAK and DYNC1H1 mRNPs (Fig. 4, B and D), even though SGs do not form. Similar compaction of the MDN1, POLA1, and PRPF8 mRNPs with puromycin treatment has been reported in HEK293T cells (Adivarahan et al., 2018).

In a third experiment, we examined the mRNP organization of AHNAK by smFISH when U-2 OS cells were treated with both arsenite and emetine (Fig. 4, E–G). If ribosome release is why mRNPs compact under stress, the addition of emetine, a drug that irreversibly blocks ribosome movement along the mRNA (Grollman, 1966), should inhibit AHNAK mRNP compaction during arsenite stress. We observed that emetine prevented AHNAK mRNP compaction during arsenite stress in U-2 OS cells (Fig. 4, E–G). Similar distances between different segments of AHNAK mRNAs were observed in cells that were not stressed versus cells that were treated with both arsenite and emetine for 60 min (Fig. 4 F). In contrast, a smaller distance between different segments of AHNAK mRNAs was observed when cells were treated with arsenite alone (Fig. 4 G). These results argue that mRNP compaction is not caused by increased macromolecular crowding found inside SGs and instead is a consequence of the loss of elongating ribosomes during translation inhibition.

Compaction of mRNPs during arsenite stress proceeds in a 5′-to-3′ direction

Because mRNP compaction is likely a consequence of ribosome release, we hypothesized that AHNAK and DYNC1H1 mRNP compaction under stress is mediated by intramolecular interactions that are formed within the ORF of mRNAs in the absence of ribosomes. If this model is accurate, mRNP compaction will begin at the 5′ end of the transcript, as elongating ribosomes translocate toward the 3′ end of the transcript once translation initiation is inhibited. This model predicts that the 5′ end to the middle of the mRNA will compact first, as elongating ribosomes move down the mRNA in the absence of new translation initiation, followed by a subsequent compaction of the middle and the 3′ end of AHNAK mRNPs as ribosomes finally exit the ORF and terminate translation. To examine this possibility, we stressed U-2 OS cells for 5, 10, 15, 20, 25, and 30 min with 500 µM arsenite and examined the distances between the different regions of the AHNAK mRNA by smFISH (Fig. 5).

Qualitatively, we observed that the distances between 5′ end and the middle are closer at 20 min after addition of arsenite, at which time the distances between the 5′ end and 3′ end or the middle and the 3′ end are still separated (Fig. 5 B). Quantitatively, the distances between the 5′ end and the middle shrink considerably after 15 min (Fig. 5 D), which correlates with the time ribosomes should be beginning to exit the 5′ portion of the coding region, taking into account that it takes 8 min after addition of arsenite to maximize eIF2α phosphorylation in U-2 OS cells (Wheeler et al., 2016). In contrast, the shrinkage in distances for the 5′ end to the 3′ end or the middle to the 3′ end is noticeable only at 25 min and significant at 30 min (Fig. 5, C and E). These results fit with the model that mRNP compaction begins at the 5′ end, as ribosomes translocate toward the 3′ end during stress.

In contrast to the arsenite time course result, we observed that all three different segments of AHNAK mRNA shrink immediately after puromycin is added (Fig. 6, B–E). Interestingly, we notice that although the distance between the 5′ and 3′ ends changes immediately with puromycin (Fig. 6 C), it keeps compacting up to 12 min after puromycin is added to cells. This differs from the changes in distances between 5′ end and middle or middle and 3′ end. This suggests that local compaction occurs at a faster rate than compaction of distant mRNA regions upon puromycin treatment (Fig. 6, C–E). These observations are consistent with the model that intramolecular folding of the mRNA, through either RNA–RNA interactions or protein binding, as ribosomes expose the coding region, leads to the increased compaction of the nontranslating mRNA.

The 5′ and 3′ ends of the AHNAK and DYNC1H1 mRNPs are closer when nontranslating

Under nonstress conditions, the 5′-to-3′ end distances of AHNAK and DYNC1H1 mRNPs are larger than one would expect based on specific models of a mRNP organization such as the closed-loop model of translation (median ∼200 nm; see Discussion). This suggests that the closed-loop model of translation either does not occur on these mRNAs or is transient. However, we noticed that the 5′ and 3′ ends of the AHNAK and DYNC1H1 mRNPs shrink disproportionally compared with the body of the mRNP under nontranslating conditions and reach a median distance between the ends of ∼50 nm (Fig. 2, E and G; Fig. 3, E and G; and Fig. 4, B and D). These results suggest that stress triggers a reorganization of mRNPs that disproportionally brings the 5′ and 3′ ends closer together.

To further examine the relationship between the 5′ and 3′ ends of these mRNAs, we measured the angles between the middle smFISH spots to the 5′ and 3′ ends for AHNAK and DYNC1H1 smFISH spots (Fig. 7 A). We observed that, in nonstress conditions,

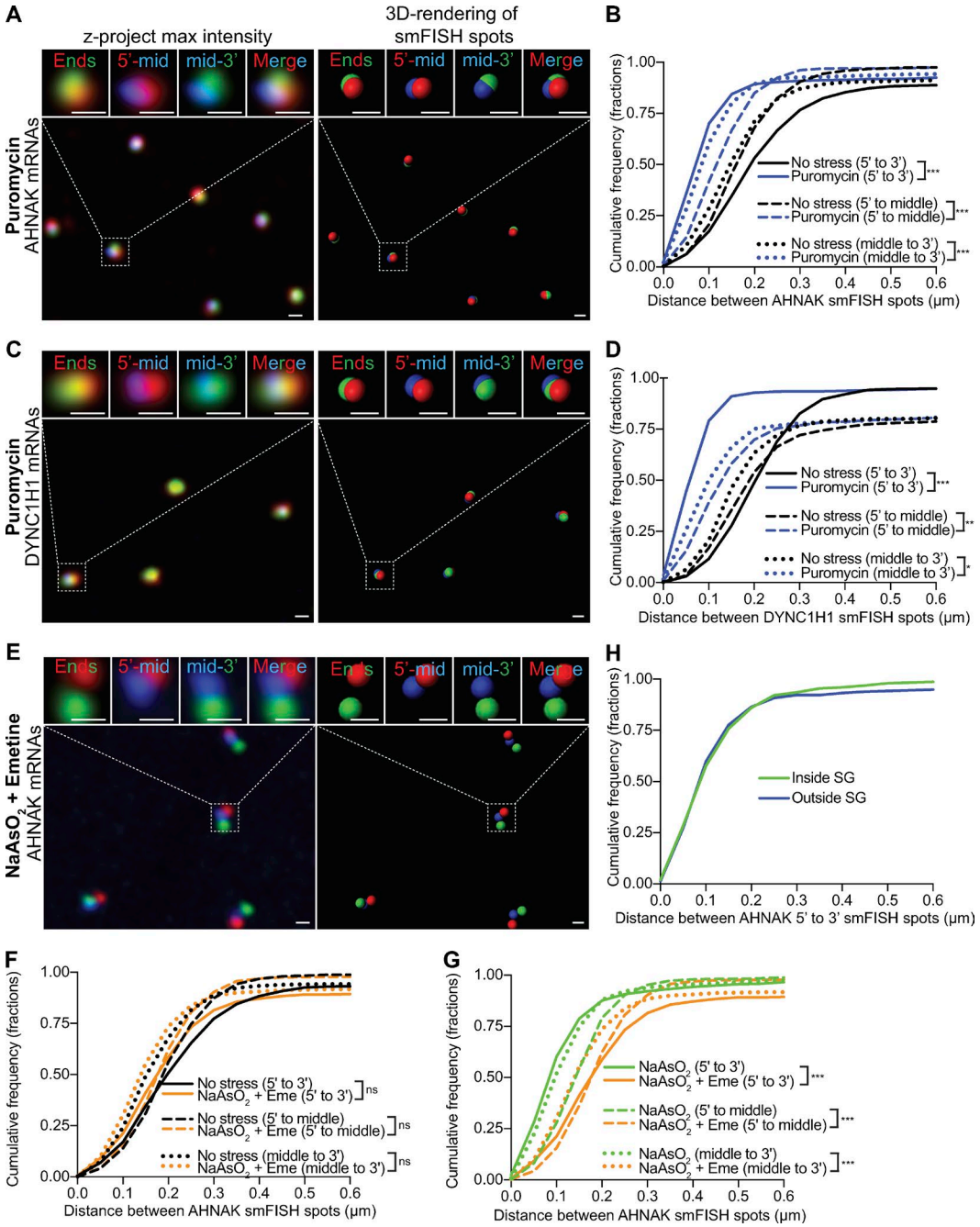

Figure 4. **Compaction of AHNAK and DYNC1H1 mRNPs correlates with ribosome release from mRNA. (A, C, and E)** Left: Representative AHNAK and DYNC1H1 smFISH images of U-2 OS cells treated with 10 µg/ml puromycin for 60 min or treated with 0.5 mM $NaAsO_2$ and 1 µM emetine (eme) for 60 min. Cells were stained with smFISH probes that bind specifically to the 5′ end (false-colored red), middle (false-colored blue), and 3′ end (false-colored green) of AHN AK and DYNC1H1 mRNAs. Right: 3D rendering of smFISH spots by Bitplane Imaris imaging analysis software. Scale bar: 250 nm. **(B, D, F, and G)** Cumulative frequency graphs (in fractions) of smallest distances between 5′ to 3′ end smFISH spots (solid lines), 5′ end to middle smFISH spots (dash lines), and middle to 3′ end smFISH spots (dotted lines) in unstressed cells (black), 10 µg/ml puromycin-treated cells (blue), 0.5 mM $NaAsO_2$-treated cells (green), and 0.5 mM $NaAsO_2$ plus 1 µM eme-treated cells (gold). More than 990 smallest distances were quantified for each sample (n = 1,107 [AHNAK puromycin], n = 992 [DYNC1H1 puromycin], n = 1,216 [nonstress, F and G], n = 999 [$NaAsO_2$, F and G], and n = 1,181 [$NaAsO_2$ plus emetine, F and G]). Scale bar: 250 nm. **(H)** Cumulative frequency graph (in fractions) of smallest distances between 5′ to 3′ end smFISH spots (solid lines) inside and outside SG in U-2 OS cells stressed with 60-min 0.5 mM $NaAsO_2$. More than 290 smallest distances were quantified (n = 550 [inside], n = 296 [outside]). The analysis was performed with the experimental results as shown in Fig. 2 (B and C). *, P ≤ 0.05; **, P ≤ 0.01; ***, P ≤ 0.001 (Student's two-tailed t test).

the angles can vary considerably, but most angles are <90°, with a median angle of ∼60° (Fig. 7, B and C). This observation suggests that these mRNAs are not linear in cells and, on average, the 5′ end is closer to the 3′ end than expected by chance, perhaps because of features of polysomes or RNA-binding proteins (see Discussion).

A striking result was that under nontranslating conditions, most angles were <45°, with a median angle of ∼20° (Fig. 7, B and

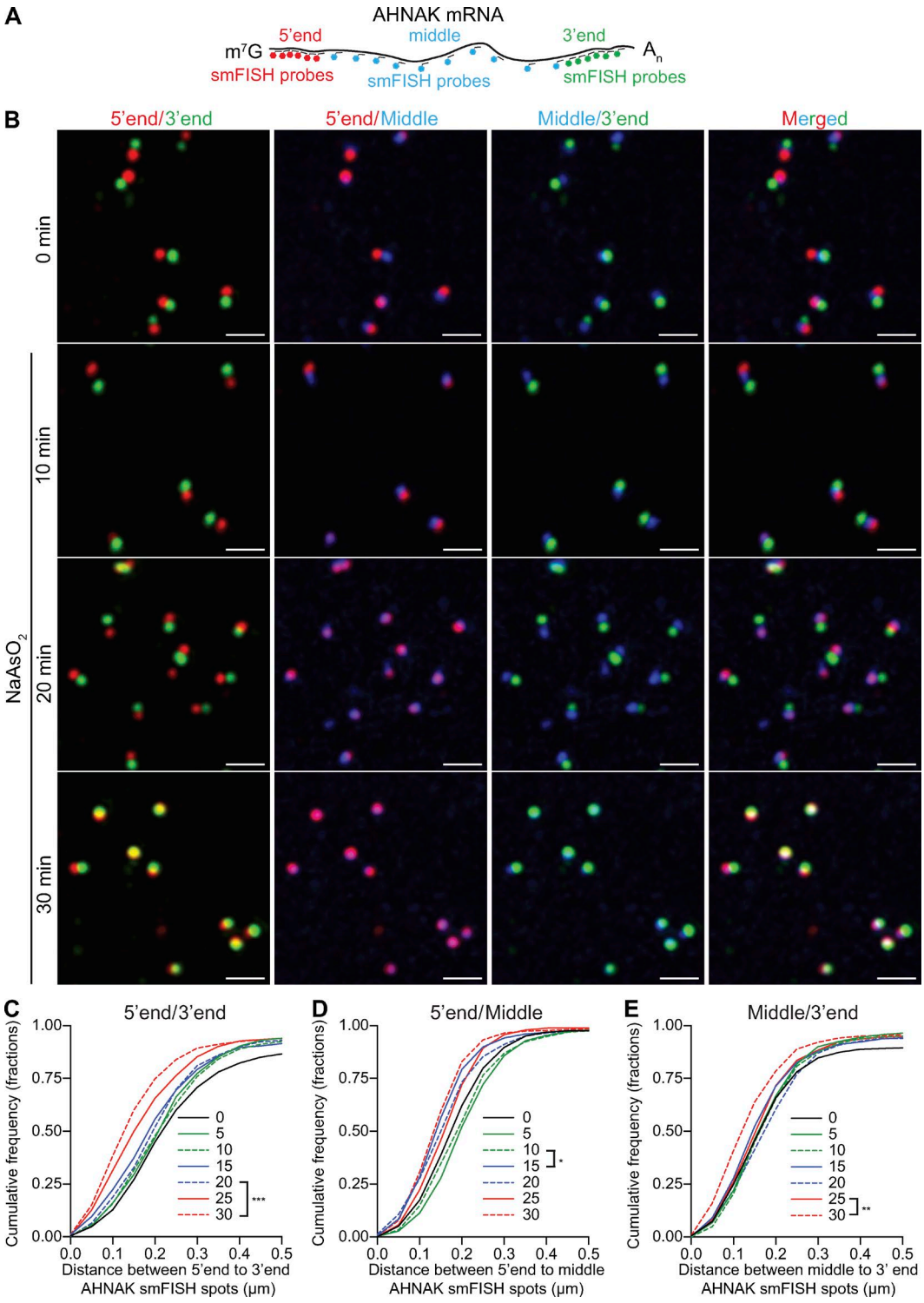

Figure 5. **Compaction of the 5′ end to the middle precedes compaction of the middle to the 3′ end during $NaAsO_2$ stress. (A)** Cartoon schematic illustrating where smFISH probes bind to AHNAK mRNAs. smFISH probes binding to the 5′ end, middle, or 3′ end are labeled with distinct fluorophores and are false-colored as red, blue, and green, respectively. **(B)** Representative AHNAK smFISH image of U-2 OS cells that were not stressed or stressed with 0.5 mM $NaAsO_2$ for 10, 20, and 30 min. Scale bar: 1 µm. **(C–E)** Cumulative frequency graphs (in fractions) of smallest distances between 5′ to 3′ end smFISH spots (C), 5′ end to middle smFISH spots (D), and middle to 3′ end smFISH spots (E) in unstressed U-2 OS cells or 0.5 mM $NaAsO_2$-treated U-2 OS cells for 5–30 min. More than 800 smallest distances were quantified for each sample (n = 1,015 [0 min], n = 954 [5 min], n = 814 [10 min], n = 952 [15 min], n = 848 [20 min], n = 915 [25 min], and n = 949 [30 min]). *, P ≤ 0.05; **, P ≤ 0.01; ***, P ≤ 0.001 (Student's one-tailed t test).

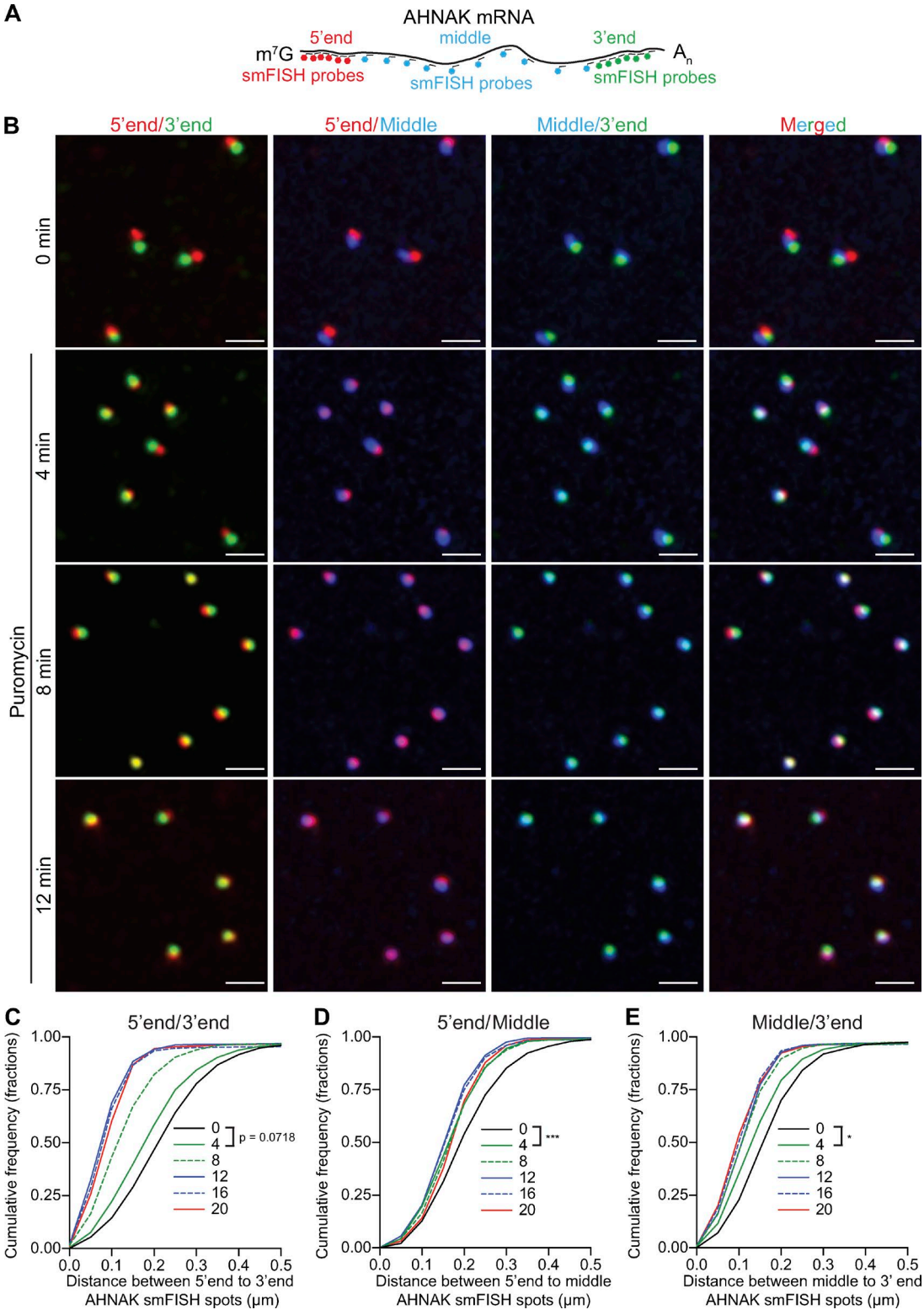

Figure 6. **Compaction of the 5′ end to the middle and compaction of the middle to the 3′ end occur simultaneously when cells are treated with puromycin. (A)** Cartoon schematic illustrating where smFISH probes bind to AHNAK mRNAs. smFISH probes binding to the 5′ end, middle, or 3′ end are labeled with distinct fluorophores and are false-colored as red, blue, and green, respectively. **(B)** Representative AHNAK smFISH image of U-2 OS cells that were not stressed or stressed with 10 µg/ml $NaAsO_2$ for 4, 8, and 12 min. Scale bar: 1 µm. **(C–E)** Cumulative frequency graphs (in fractions) of smallest distances between 5′ to 3′ end smFISH spots (C), 5′ end to middle smFISH spots (D), and middle to 3′ end smFISH spots (E) in unstressed U-2 OS cells or puromycin-treated U-2 OS cells for 4–20 min. More than 1,000 smallest distances were quantified for each sample (n = 1,037 [0 min], n = 1,383 [4 min], n = 1,183 [8 min], n = 1,166 [12 min], n = 1,014 [16 min], and n = 1,134 [20 min]. *, P ≤ 0.05; ***, P ≤ 0.001 (Student's one-tailed t test).

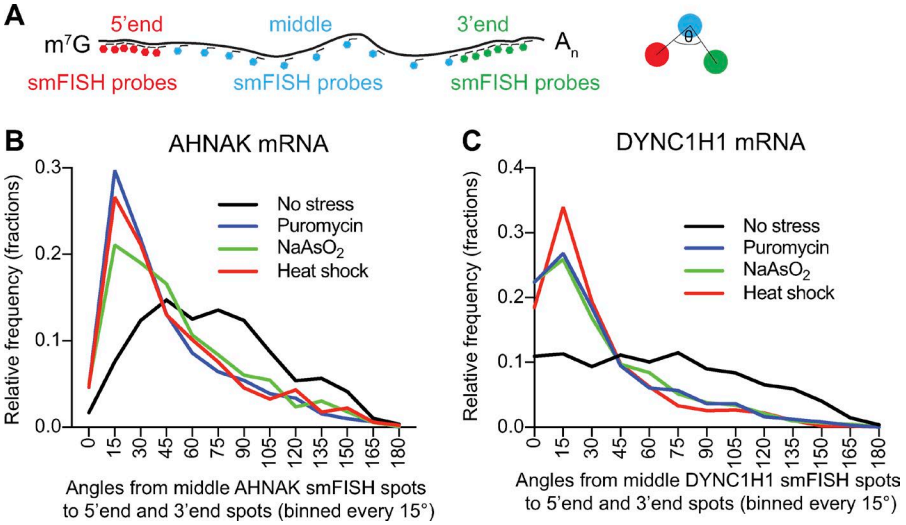

Figure 7. **Translation inhibition with puromycin, $NaAsO_2$, or heat shock in U-2 OS cells disproportionally shrink the distances between the 5′ and 3′ ends relative to the middle of AHNAK and DYNC1H1 mRNPs. (A)** Cartoon schematic indicating the angles that were measured in B and C. **(B and C)** Histograms illustrating the relative frequency (fractions) of angles from middle smFISH spots to 5′ end and 3′ end smFISH spots of AHNAK (B) and DYNC1H1 (C) mRNAs in unstressed (black line), puromycin-treated (blue), $NaAsO_2$-treated (green), or heat shocked (red) U-2 OS cells. The histograms were generated by binning every 15°. For AHNAK, more than 850 angles were quantified for each sample (n = 1,189 [no stress], n = 1,062 [$NaAsO_2$], n = 860 [heat shock], and n = 1,107 [puromycin]). For DYNC1H1, more than 1,000 angles were quantified for each sample (n = 1,113 [no stress], n = 1,032 [$NaAsO_2$], n = 1,056 [heat shock], and n = 992 [puromycin]).

C). Because the mRNAs were compact under these conditions, we were concerned that the small spacing between the smFISH spots might skew this analysis. Given this, we performed a second analysis in which we limited our analysis to specific mRNAs where the total distance between the 5′ end to middle and the middle to 3′ end is between 0.3 and 0.6 µm, with the goal of increasing our ability get an accurate angle measurement. This analysis also showed a dramatic reduction in the angle between the 5′-middle-3′ signals (Fig. S5). This provides a second line of evidence that when mRNAs exit translation, the distance between the 5′ and 3′ ends of AHNAK and DYNC1H1 mRNPs is notably compacted, perhaps because of the polymer nature of the mRNA (see Discussion).

The distance between the 5′ and 3′ ends of SunTagx32-DYNC1H1 reporter mRNAs are longer when engaged in translation

The above results show a correlation between mRNP architecture based on the expected translation status of the mRNAs. To directly examine the architecture of translating and nontranslating mRNAs, we obtained HeLa cells stably expressing SunTagx32-DYNC1H1 and single-chain variable fragment (scFv)–GFP (Xavier Pichon and Edouard Bertrand, Institut de Génétique Moléculaire de Montpellier, Montpellier, France; Pichon et al., 2016). This cell line allows us to simultaneously monitor DYNC1H1 mRNA engaged in translation in a single-molecule manner by detecting the 32 copies of the SunTag in the nascent peptide, while the architecture of the same mRNA can be determined by smFISH (Fig. 8 A). The bright scFv-GFP foci (false-colored as gray) as documented by Pichon et al. (2016) and confirmed here are SunTagx32-DYNC1H1 mRNAs engaged in translation because they are sensitive to translation inhibition by puromycin or arsenite (Fig. 8 B). Moreover, corresponding SunTag and DYNC1H1 3′ end smFISH spots are almost always observed in proximity to the bright scFv-GFP foci (false-colored in blue) in nonstress conditions (Fig. 8 D). We observed that the 5′ and 3′ ends are further apart when SunTagx32-DYNC1H1 mRNAs are engaged in translation compared with cells treated with puromycin, where we observe the nascent peptide is released from the mRNAs (Fig. 8, B, D, and E). These results directly demonstrate that translating mRNAs are less compact than mRNAs that have been released from ribosomes.

mRNA compaction is ATP independent

In principle, mRNA compaction could be driven by RNA–RNA interactions and be independent of any energy input. Alternatively, mRNA compaction after ribosome release could require energy input, perhaps through the action of specific helicases. Previous results have shown that ATP depletion blocks SG formation (Jain et al., 2016), which could be caused by a defect in ribosome release or mRNP remodeling. To examine the role of ATP in mRNA compaction, we first asked how ATP depletion affects ribosome release after inhibition of translation initiation. For this experiment, we depleted ATP from cells using 2-deoxyglucose (2DG) and carbonyl cyanide m-chlorophenyl hydrazone (CCCP; Jain et al., 2016) and examined whether the SunTagx32-DYNC1H1 mRNA maintained its association with ribosomes during arsenite stress as assessed by the presence of the nascent peptide chain. Arsenite treatment alone caused the SunTagx32-DYNC1H1 mRNA to lose its association with nascent chains, as expected from ribosome runoff (Fig. 8 B). In contrast, in cells depleted for ATP, the SunTagx32-DYNC1H1 mRNA maintained its association with nascent chains even after arsenite treatment (Fig. 8 C). This is consistent with ribosome elongation and release requiring energy and provides a molecular explanation for why ATP depletion limits SG formation (Jain et al., 2016).

To determine whether ATP depletion could affect mRNA compaction directly, we used puromycin to release ribosomes independently of elongation. In ATP-depleted cells, puromycin was still effective at releasing nascent chains from the SunTagx32-DYNC1H1 mRNA (Fig. 8 C). Moreover, even when ATP was depleted, the SunTagx32-DYNC1H1 mRNA compacted to the same extent as seen in the presence of ATP (Fig. 8, F and G). Thus, mRNA compaction following ribosome release is independent of energy.

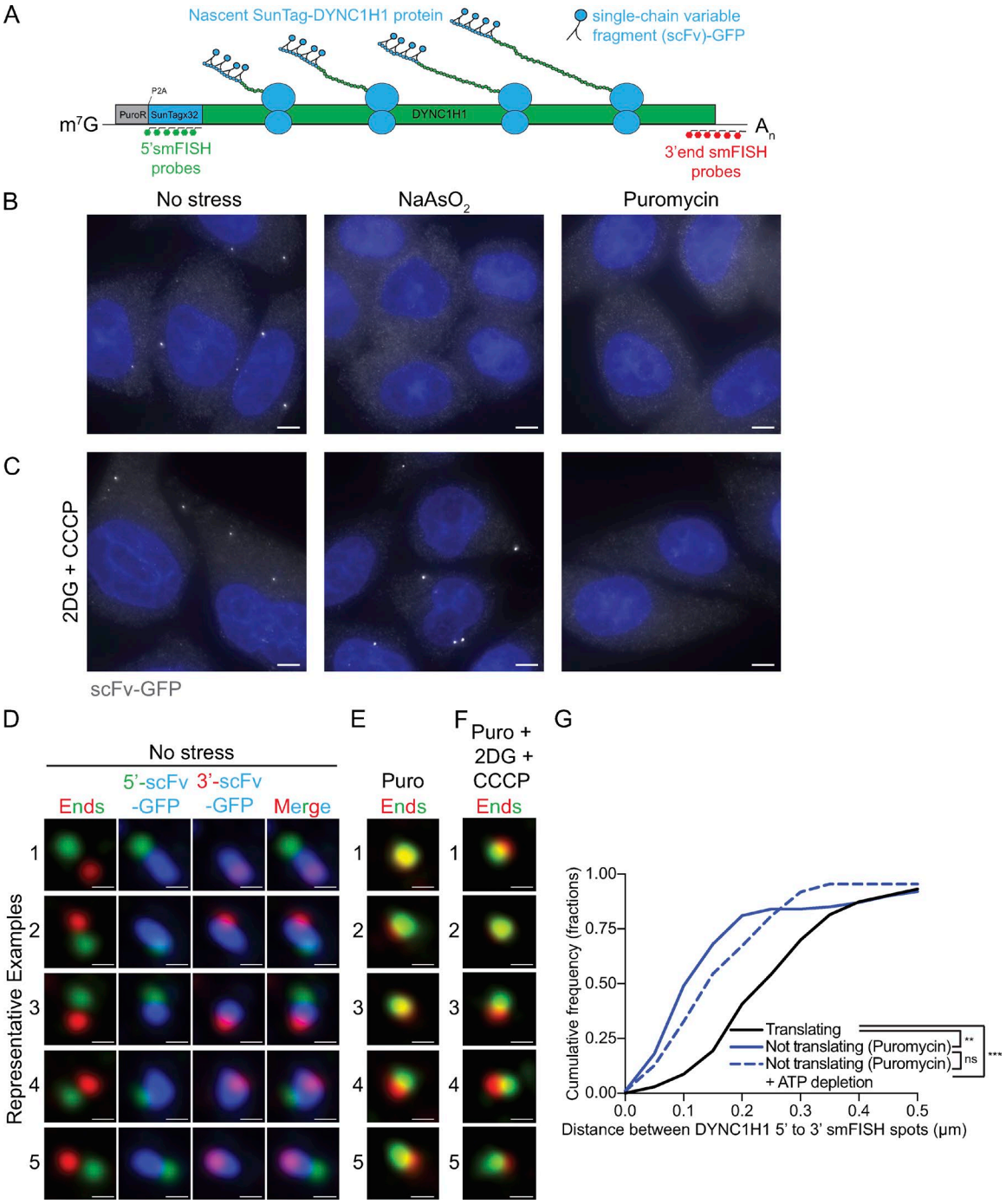

Figure 8. **Distances between SunTagx32-DYNC1H1 mRNAs 5′ and 3′ ends are larger when engaged in translation than when it is not. (A)** Cartoon schematic illustrating where smFISH probes bind to SunTagx32-DYNC1H1 single-molecule translation reporter. The smFISH probes binding to the 5′ end and 3′ end are false-colored as green and red, respectively, and the scFv-sfGFP antibody is false-colored as blue. The SunTagx32-DYNC1H1 reporter and the scFv-sfGFP are stably expressed in HeLa cells. **(B and C)** Representative images of HeLa cells stably expressing SunTagx32-DYNC1H1 and scFv-sfGFP (false-colored gray) treated with $NaAsO_2$ for 60 min or puromycin for 30 min without (B) or with (C) 2DG and CCCP. Middle (C): 2DG, CCCP, and $NaAsO_2$ were added at the same time to the cells and incubated for 60′. Right (C): 2DG and CCCP were added first to cells for 30 min before adding puromycin to the cells and incubated for another 30′. Cells were stained with DAPI (false-colored blue). Scale bar: 5 µm. **(D–F)** Representative images of individual SunTagx32-DYNC1H1 reporter RNA (false-colored blue) and stained with SunTagx32-specific (false-colored green) and 3′ end DYNC1H1 smFISH probes (false-colored red) in HeLa cells unstressed (D) or treated with puromycin (E), or puromycin, 2DG, and CCCP (F). Scale bar: 250 nm. **(G)** Cumulative frequency graph (in fractions) of smallest distances between 5′ to 3′ end smFISH spots in unstressed HeLa cells with a corresponding scFv-sfGFP fluorescent spot (black line) and puromycin-treated or puromycin (blue-line), 2DG-, and CCCP-treated HeLa (blue dashed line). At least 100 smallest distances were quantified for each sample (n = 103 [translating], n = 100 [not translating], and n = 110 [puromycin + 2DG + CCCP]. **, P ≤ 0.01; ***, P ≤ 0.001 (Student's two-tailed t test).

Discussion

mRNAs need to exit translation completely before entering SGs

We present several observations that indicate mRNAs must be completely disengaged from translating ribosomes before entering SGs (Fig. 9). First, mRNAs with long ORFs are slower at recruitment to SGs than mRNAs with short ORFs (Fig. 1, A and B; and Fig. S1). Second, recruitment of mRNAs with long ORFs to arsenite-induced SGs is quicker when puromycin is added, which will rapidly disengage elongating ribosomes (Fig. 1, A and C; and Fig. S2). Third, addition of cycloheximide to cells treated with arsenite for 30 min inhibits additional recruitment of RNA to SGs (Fig. 1, A and D; and Fig. S3), which indicates that the continued accumulation of AHNAK and DYNH1C1 mRNAs to SGs requires ribosome runoff. For mRNAs with long ORFs such as AHNAK and DYNH1C1, a large amount of the ORF will be exposed by 30 min of stress, yet only a small percentage of these mRNAs accumulate in SGs at that time. This argues that mRNAs must fully disengage from elongating ribosomes before stable accumulation in SGs. Additional evidence in support of this model comes from single-molecule experiments showing that mRNAs engaged with ribosomes can form only a transient association with SG and do not enter a stable association, which can be seen with nontranslating mRNAs (Moon et al., 2018 *Preprint*).

It is an unsolved mystery why complete ribosome disengagement is required for stable association of mRNAs with SG. One possibility is that the mRNA association with the translation machinery increases the presence of helicases and/or protein chaperones that prevent or disengage interactions between the translating mRNP and SG. Alternatively, it may be energetically unfavorable for an 80S ribosome and its associated factors to enter the altered environment of a SG, either because of energetic costs of changes in solvation, or because the mesh size of an SG is smaller than an assembled 80S ribosome.

mRNPs are compact in both translating and nontranslating states

We present several observations that demonstrate mRNAs are compacted >10-fold relative to their contour length even when they are translating. First, under no stress conditions, the median distances between the 5′ and 3′ end of AHNAK and DYNC1H1 mRNPs are roughly ∼200 nm (Figs. 2 C, 3 C, and 8 D). Relative to the AHNAK and DYNC1H1 mRNAs' contour lengths, 5.6 and 4.2 µm respectively, this is ∼28- and ∼21-fold compaction, respectively. Second, the median distances between the 5′ and middle or 3′ and middle of AHNAK and DYNC1H1 are roughly ∼150 nm (Figs. 2 C and 3). Relative to half of its contour length, this is ∼19- and ∼14-fold compaction. Third, we notice that the angles between the middle and the 5′ and 3′ end of AHNAK and DYNC1H1 mRNPs are usually <90° (Fig. 7, B and C; and Fig. S5, B and C), which also suggests significant compaction of the ends relative to the linear length. Similar results are seen for the MDN1, POLA1, and PRPF8 mRNAs in HEK293 cells, indicating this is a general phenomenon (Adivarahan et al., 2018).

We suggest two mechanisms to account for the compaction of mRNAs during nonstress conditions. First, we suggest that transient folding of the ORF region between elongating ribosomes compacts mRNAs (Fig. 9). The average interribosome distance is estimated to be 150 nucleotides in yeast and 189 in mammalian cells (Arava et al., 2003; Hendrickson et al., 2009), or from single-molecule translation assays in mammalian cells, the average interribosome distance is estimated to be between 200 and 900 nucleotides (Morisaki et al., 2016; Wang et al., 2016; Wu et al., 2016; Yan et al., 2016). Additionally, for DYNC1H1 mRNPs specifically, it is estimated that on average each DYNC1H1 mRNA has approximately seven ribosomes (Pichon et al., 2016). Because a ribosome footprint is ∼30 nucleotides (Steitz, 1969; Wolin and Walter, 1988), this suggests that most of the nucleotides in the ORF are not covered with ribosomes. We estimate that ∼80–98% of the ORF nucleotides for most mRNAs, and ∼98% for DYNC1H1 mRNA, are not engaged with ribosomes. Therefore, the ORF region can form significant intramolecular interactions with itself, or with the 5′ and 3′ UTRs. Supporting this model, an extensive physical association between the 3′ UTR and the ORF has been reported for mRNAs (Eldad et al., 2008). Compaction of mRNAs caused by intramolecular RNA–RNA interactions is also consistent with our observation that compaction occurs even in ATP-depleted cells (Fig. 8). Besides intramolecular interactions, the folding of the ORF region may be promoted by RNA-binding proteins or complexes by connecting different ORF regions of the mRNA.

A second mechanism of compacting translating mRNAs may arise from the architecture of polysomes, because the path a mRNA takes within each ribosome is curved (Agrawal et al., 1996). Therefore, by its nature, a translating mRNA would be more compact compared with its contour length. Indeed, instances of circular, spiral, rosette, staggered line, double-row, and helical polysomes have been observed by traditional EM or more advanced cryo-EM and cryo-ET methods, all of which would compact the overall shape of the mRNA (Palade, 1955; Warner et al., 1962; Wettstein et al., 1963; Daneholt et al., 1977; Yazaki et al., 2000; Madin et al., 2004; Kopeina et al., 2008; Brandt et al., 2009, 2010; Afonina et al., 2013, 2014, 2015; Myasnikov et al., 2014; Viero et al., 2015).

We and others (Adivarahan et al., 2018) observe that, under stress conditions, when mRNAs stop translating, mRNPs compact further (Fig. 9). Specifically, the distances between the 5′ to 3′ ends, 5′ end to the middle, and 3′ end to the middle are smaller for AHNAK and DYNC1H1 mRNAs under a variety of conditions that cause mRNAs to disengage from elongating ribosomes, such as arsenite, heat-shock, and puromycin but not emetine (Figs. 2, 3, and 4). This additional compaction appears to be a consequence of translational shutoff and not a consequence of being inside SGs for two reasons (Fig. 9). First, compaction is similar inside and outside SGs (Fig. 4 H). Second, puromycin treatment also compacts AHNAK and DYNC1H1 mRNPs without inducing SGs (Fig. 4, A–D). The most straightforward interpretation for increased mRNP compaction during stress is mRNAs forming increased intramolecular interactions in the absence of translating ribosomes. This interpretation is supported by the fact that the compaction precedes temporally in a 5′-to-3′ manner that correlates with ribosomes transiting toward the 3′ end of AHNAK mRNAs after the addition of arsenite (Fig. 5).

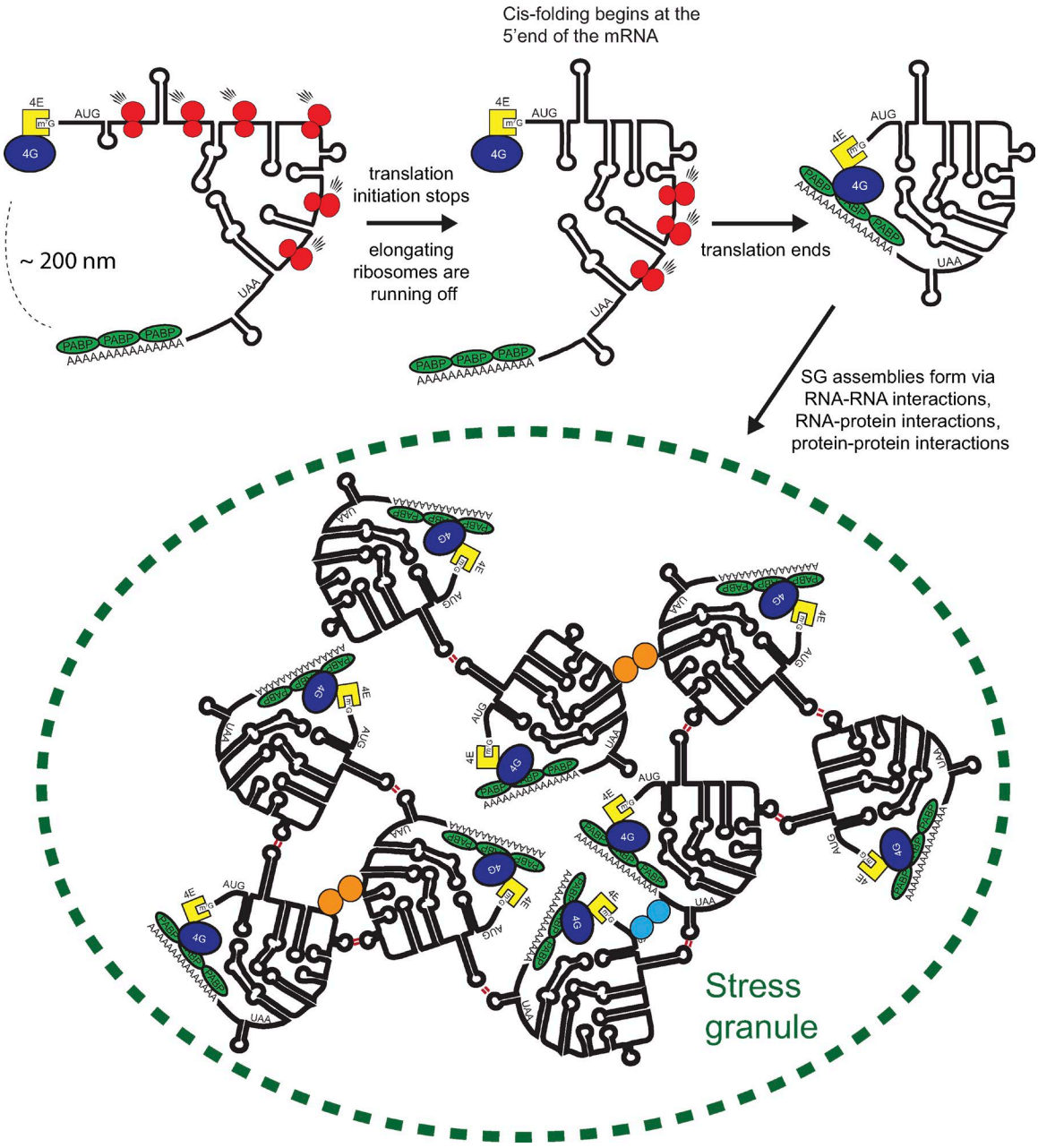

Figure 9. **Model depicting mRNP compaction and mRNA recruitment to SGs.** Under nonstress conditions, mRNPs are engaged in translation. Relative to its contour length, significant compaction was observed. During the early stages of stress, ribosomes will migrate toward the 3′ end of mRNAs and mRNAs start to compact at the 5′ end, most likely because of intramolecular interactions formed. When mRNA exits translation, the mRNP compacts further and the ends are disproportionally close. One hypothesis is the closed-loop conformation is reestablished. Some of these mRNPs, preferentially long mRNAs, start to accumulate in SGs via intermolecular interactions formed with other mRNPs.

The spatial relationship between the 5′ and 3′ ends changes with stress

We observed that mRNPs are reorganized during stress in a manner in which the distances between the ends are now smaller than the distances between the ends to the middle for AHNAK and DYNC1H1 mRNAs (Fig. 9). Specifically, the median distance between the 5′ and 3′ end is ∼50 nm during stress, whereas the median distance between the 5′ end to the middle or 3′ end to the middle is ∼100 nm (Fig. 2, E and G; Fig. 3, E and G; and Fig. 4, B and D). This is different with respect to translating mRNPs; the median distance between the ends (∼200 nm) is larger than the median distance between the 5′ end or 3′ end to the middle (∼150 nm; Figs. 2 C and 3 C). In support of the 5′ and 3′ ends being in proximity under stress, we also observed that the angles between the middle and the ends of AHNAK and DYNC1H1 mRNAs are now considerably smaller under stress (Fig. 7, B and C; and Fig. S4, B and C).

We suggest two possible mechanisms for why the 5′ and 3′ ends may enter closer proximity during stress. One hypothesis is that the closed-loop conformation is a nonstable state during translation and that in the absence of translation, the closed loop conformation can form through interactions of eIF4E, eIF4G, and

PABP where eIF4E binds to the m^{7}G cap, PABP binds to poly(A) tail, and eIF4G binds to both eIF4E and PABP (Hinnebusch and Lorsch, 2012; Fig. 9). Alternatively, or in addition, the 5′ and 3′ ends of mRNPs may be close during stress because of an intrinsic property of "naked" RNAs to fold in a manner that brings the ends in proximity. Several computation studies suggest that the ends of mRNAs are close (<10 nm) for RNAs in solution (Fang et al., 2011; Yoffe et al., 2011; Clote et al., 2012). Moreover, an in vitro FRET-based assay indicates that for all 11 mRNAs examined, the distance between the 5′ and 3′ ends is <10 nm (Lai et al., 2018 *Preprint*). This distance is significantly smaller than one would expect if it these RNAs were behaving as a random coil in solution (Lai et al., 2018 *Preprint*). Therefore, under stress conditions, if most mRNAs are now exposed and can form significant intramolecular interactions, the properties of RNA as a polymer might promote the interaction of the 5′ and 3′ ends.

To consider whether there could be a direct interaction between the 5′ and 3′ ends of mRNAs at the distances estimated from our smFISH analysis, we estimated what distance we would observe by smFISH for a classic eIF4E-eIF4G-PABP closed-loop structure (Fig. S5). In a closed-loop model with PABP interacting with eIF4G, the distance between the m^{7}G-cap and the poly(A) tail ends should be <20 nm, because the diameter of an average protein is ∼3–6 nm (Milo et al., 2010). We estimate the distance between the m^{7}G-cap and the last nucleotide that precedes the poly(A) tail to be ∼50 nm, because the average poly(A)-tail of a mammalian mRNA is <100 nucleotides (Chang et al., 2014), and when fully extended is ∼30 nm in length (Milo et al., 2010). Finally, given where the 5′ and 3′ end smFISH probes bind on AHNAK and DYNC1H1 mRNAs, and provided if the overall compaction of AHNAK and DYNC1H1 mRNAs is similar at the ends (>20 fold), we estimate that a distance <80–65 nm between 5′ end and 3′ end of AHNAK and DYNC1H1 smFISH spots, respectively, could support a closed-loop conformation (Fig. S5). Although these calculations should be taken as ballpark estimates, they would suggest that <20% of AHNAK and DYNC1H1 translating mRNPs have distances between the ends supporting a closed-loop conformation. In contrast, during stress, when mRNAs exit translation, >50% of AHNAK and DYNC1H1 mRNAs have distances that are consistent with the closed-loop conformation (Fig. 2, E and G; Fig. 3, E and G; and Fig. 4, B and D). Similar results have also been described for the MDN1, POLA1, and PRPF8 mRNAs (Adivarahan et al., 2018), suggesting that this effect is not limited to the mRNAs we have examined. Thus, one mechanism for the shortened distance between the 5′ and 3′ ends during stress could be direct protein–protein interactions (Fig. 9).

The observation that the distances between the ends of translating mRNPs are typically large (greater than 100 nm) is surprising with respect to many aspects of established RNA biology. For example, the closed-loop model is consistent with the observations that the poly(A) tail, and other 3′ UTR regulatory elements, can affect processes occurring at the 5′ UTR (e.g., miRNA-mediated translation initiation repression). Our observations suggest that this is not physically possible for translating mRNPs unless there is a large network of protein–protein interactions that connect the ends (>20 proteins, because an average protein diameter is ∼3–6 nm). Alternatively, we hypothesize, based on observations derived from nontranslating conditions, that effects imparted by 3′ UTR regulatory elements on processes at the 5′ end will occur only when all translating ribosomes are released from the mRNA. If this is accurate, it suggests that translating mRNAs are likely unaffected by these 3′ UTR regulatory elements. However, when an mRNA loses all its translating ribosomes, most likely in a stochastic manner, these regulatory elements can now communicate with the 5′ end and affect mRNA fate. This leads to a model wherein 3′ UTR elements can affect events at the 3′ end of the mRNA, such as deadenylation, regardless of translation status, but the ability of the 3′ UTR and poly(A) tail to influence events at the 5′ mRNA end, such as translation initiation and decapping, would be more pronounced on mRNAs that have exited translation.

Materials and methods

U-2 OS and HeLa cells growth conditions

Human osteosarcoma U-2 OS cells (Kedersha et al., 2016), maintained in DMEM with high glucose, 10% FBS, and 1% penicillin/streptomycin at 37°C/5% CO_2, were used in most experiments (Figs. 1, 2, 3, 4, 5, 6, and 7; and Figs. S1, S2, S3, and S4). HeLa cells stably expressing SunTagx32-DYNC1H1 and the scFv-sfGFP (Pichon et al., 2016; Fig. 8) were also maintained in DMEM with high glucose, 10% FBS, and 1% penicillin/streptomycin at 37°C/5% CO_2.

Sequential immunofluorescence and single-molecule FISH

The protocol was performed as described previously (Khong et al., 2017, 2018). Briefly, U-2 OS or HeLa cells were seeded on sterilized coverslips in six-well tissue culture plates. At ∼80% confluence, medium was exchanged 60 min before experimentation with fresh medium. Experimentation was performed as indicated in each figure. U-2 OS and HeLa cells stably expressing SunTagx32-DYNC1H1 and scFv-sfGFP were treated with 500 µM $NaAsO_2$, 10 µg/ml puromycin, 1 µM emetine, or 50 µg/ml cycloheximide. ATP was depleted by treating HeLa cells with 200 mM 2DG and 100 µM CCCP. After treating the cells, the medium was aspirated, and the cells were washed with prewarmed 1× PBS. The cells were then fixed with 500 µl of 4% paraformaldehyde for 10 min at room temperature.

After fixation, cells were washed twice with PBS, permeabilized in 0.1% Triton X-100 and PBS for 5 min, and washed once with PBS. Coverslips were transferred to a humidifying chamber and incubated in 5 µg/ml mouse α-G3BP1 antibody in PBS (ab56574; Abcam) for 60 min at room temperature. After incubation, the coverslips were transferred to a new six-well plate and washed three times with PBS. Coverslips were then transferred back to the humidifying chamber and incubated in goat α-mouse FITC-conjugated antibody in PBS (1:1,000 dilution; ab6785; Abcam) for 60 min at room temperature. The coverslips were transferred to a six-well plate and washed three times with PBS. Antibodies were then fixed on the cells by incubating coverslips with 500 µl of 4% paraformaldehyde for 10 min at room temperature.

After staining the cells with antibodies, smFISH was performed as described previously (Khong et al., 2018) using Biosearch

Technologies Stellaris buffers (SMF-HB1-10, SMF-WA1-60, and SMF-WB1-20). Specific smFISH probes were created using the Stellaris Probe Designer software designed by Biosearch Technologies. smFISH probes that bind to DYNC1H1, NORAD, PEG3, ZNF704, CDK6, and the 5′ and 3′ ends of AHNAK mRNAs were designed previously (Khong et al., 2017; Moon et al., 2018 *Preprint*). Newly designed smFISH probes include probes that bind to the middle of AHNAK mRNAs, 5′ end, middle, 3′ end, and SunTag DYNC1H1 mRNAs. These smFISH probes were made by conjugating 30 to 60 DNA oligos with ddUTP-Atto488, ddUTP-Atto550, or ddUTP-Atto633 as described in Gaspar et al. (2017; Table S1). ddUTP-Atto633 was a gift from Anne Ephrussi's lab (European Molecular Biology Laboratory, Heidelberg, Germany). CDK6 smFISH probes conjugated to Atto633 were made by Evan Lester in the Parker Lab (University of Colorado Boulder, Boulder, CA).

Imaging parameters

Fixed and stained U-2 OS and HeLa cells were imaged using a GE wide-field DeltaVision Elite microscope with an Olympus UPlanSApo 100×/1.40-NA Oil Objective lens and a PCO Edge sCMOS camera with appropriate filters at room temperature by SoftWoRx Imaging software as described previously (Khong et al., 2018). At least 25 Z-sections (0.2-µm step size) were captured for each image to include the entire cell. Imaging parameters were adjusted to capture fluorescence within the scope's dynamic range. After image collection, the images were deconvolved with built-in DeltaVision SoftWoRx Imaging software (method, enhanced ratio [aggressive]; number of cycles, 10; and noise filtering, medium [200 nm]) as described previously (Khong et al., 2018). Images shown in the manuscript are Z-stacked by ImageJ (National Institutes of Health) with Fiji plugin and were adjusted by brightness and contrast accordingly to best illustrate results. All images shown are deconvolved except for Fig. 8 (B and C).

Image analysis

All image analysis was performed using Bitplane Imaris image analysis software as described previously with the deconvolved images (Khong et al., 2018). To measure the fraction of smFISH spots in SGs in U-2 OS cells, please refer to Khong et al. (2018).

We quantified the distances between the 5′ end, middle, and 3′ end of AHNAK and DYNC1H1 mRNAs with the help of Bitplane Imaris Imaging Analysis software in the following manner. (1) We load the deconvolved DeltaVision images in Bitplane Imaris Imaging Analysis Software (see imaging parameters), which reconstitutes each focal plane in 3D automatically. (2) We mask all fluorescent signal coming from the nuclei of cells of an image by using DAPI staining to define the nuclei. (3) We apply the spot creation wizard to identify the 5′ end, middle, and 3′ end AHNAK and DYNC1H1 smFISH spots using two parameters: a fixed xy-diameter spot size of 200 nm and a manually determined fluorescent quality threshold. Upon identification of smFISH spots, the spot creation wizard provides all x,y,z coordinates for the center of each smFISH spot which, we export as an Excel file. (4) We export the coordinates of all smFISH spots and compute the distances between all smFISH spots in different channels by applying the distance formula between two points in 3D space. (5) We note the smallest distance between all smFISH spots of different channels. We assume that the smallest distance is the distance between two regions of a single AHNAK or DYNC1H1 mRNA molecule. (6) Last, any ambiguity in assigning all three smFISH spots to the same RNA is excluded from the analysis. With respect to angle measurements (Figs. 7 and S4), with the smallest distances between smFISH spots provided as described above, we compute the angles between the middle smFISH spots to the 5′ and 3′ end smFISH spots by applying the law of cosines with three known sides.

The method used to quantify the distances between the 5′ Suntag smFISH spot and the 3′ end DYNC1H1 spot in Fig. 8 is identical to the approach described in the previous paragraph except for two key differences. (1) The distance is measured between the 5′ and 3′ end smFISH spots only when a corresponding scFv-GFP spot is identified in nonstress samples (Fig. 8 G; <2 µm away from 5′ Suntag fluorescent spot). (2) In addition, distances between the 5′ and 3′ end that are larger than 1 µm are not included in the analysis (Fig. 8 G). The exclusion of data was applied because without a third smFISH (middle), there is ambiguity about whether the two spots are from the same RNA. 1 µm distance was chosen as a cutoff because the distances between the ends of DYNC1H1 mRNA was almost always <1 µm in nonstress and stress conditions (Figs. 3 and 4).

Statistical analysis

Statistical analysis was performed using Prism 7 for Mac OS. One-tailed binominal distribution was applied in Fig. 1 for individual RNAs between U-2 OS cells treated for 30 min with $NaAsO_2$ versus U-2 OS cells treated for 30 min with $NaAsO_2$ and puromycin; the *p*-values are indicated in the text. Statistical analysis was performed in Figs. 2, 3, 4, 5, and 6 by applying Student's *t* tests. Two-tailed Student's *t* test was performed in Figs. 2, 3, 4, and 8. One-tailed Student's *t* test was performed in Figs. 5 and 6 because we expected the distance to shrink with arsenite and puromycin overtime as described in Figs. 2, 3, and 4.

Online supplemental material

Figs. S1, S2, and S3 are representative images of the quantified results shown in Fig. 1. Some images shown in Fig. 1 are the zoomed-in images shown in Figs. S1, S2, and S3. Fig. S4 shows that the ends of AHNAK and DYNC1H1 mRNAs disproportionally shrink relative to the middle segments when U-2 OS cells are stressed. This is similar to Fig. 7, except the analysis was restricted to distances of 0.3–0.6 µm between 5′ end to middle and middle to 3′ end smFISH spots. Fig. S5 is a cartoon schematic of distances between 5′ and 3′ end smFISH spots AHNAK and DYNC1H1 mRNAs that we estimate to be consistent with the closed-loop translation model. Table S1 lists the DNA oligo sequences that were used to make smFISH probes.

Acknowledgments

We thank Xavier Pichon and Edouard Bertrand for the HeLa cell line stably expressing SunTagx32-DYNC1H1 and scFv-sfGFP, Nancy Kedersha and Paul Anderson for the U-2 OS cells, Anne Ephrussi for providing ddUTP-Atto633, and Evan Lester for making CDK6 smFISH probes. We thank Carolyn Decker for DeltaVision training, and

we are grateful to Joe Dragavon for image analysis training (Bitplane Imaris Image Analysis Software). The imaging data analysis was performed at the University of Colorado BioFrontiers Institute Advanced Light Microscopy Core. We thank Theresa Nahreini for the cell culture facility training (BioFrontiers Cell Culture Facility), Briana Van Treeck and Carolyn Decker for careful reading of the manuscript, and Olke C. Uhlenbeck for helpful discussion.

This work was funded by the Howard Hughes Medical Institute (R. Parker). A. Khong is supported by a Banting Postdoctoral Fellowship.

The authors declare no competing financial interests.

Author contributions: A. Khong conceived and performed experiments, analyzed results, and contributed to manuscript preparation. R. Parker contributed to project conception and manuscript preparation.

Submitted: 26 June 2018
Revised: 5 September 2018
Accepted: 4 October 2018

References

Adivarahan, S., N. Livingston, B. Nicholson, S. Rahman, B. Wu, O. Rissland, and D. Zenklusen. 2018. Spatial organization of single mRNPs at different stages of the gene expression pathway. *Mol. Cell*. https://doi.org/10.1016/j.molcel.2018.10.010

Afonina, ZhA., A.G. Myasnikov, N.F. Khabibullina, A.Y. Belorusova, J.F. Menetret, V.D. Vasiliev, B.P. Klaholz, V.A. Shirokov, and A.S. Spirin. 2013. Topology of mRNA chain in isolated eukaryotic double-row polyribosomes. *Biochemistry (Mosc.)*. 78:445–454. https://doi.org/10.1134/S0006297913050027

Afonina, Z.A., A.G. Myasnikov, V.A. Shirokov, B.P. Klaholz, and A.S. Spirin. 2014. Formation of circular polyribosomes on eukaryotic mRNA without cap-structure and poly(A)-tail: a cryo electron tomography study. *Nucleic Acids Res.* 42:9461–9469. https://doi.org/10.1093/nar/gku599

Afonina, Z.A., A.G. Myasnikov, V.A. Shirokov, B.P. Klaholz, and A.S. Spirin. 2015. Conformation transitions of eukaryotic polyribosomes during multi-round translation. *Nucleic Acids Res.* 43:618–628. https://doi.org/10.1093/nar/gku1270

Agrawal, R.K., P. Penczek, R.A. Grassucci, Y. Li, A. Leith, K.H. Nierhaus, and J. Frank. 1996. Direct visualization of A-, P-, and E-site transfer RNAs in the Escherichia coli ribosome. *Science.* 271:1000–1002. https://doi.org/10.1126/science.271.5251.1000

Arava, Y., Y. Wang, J.D. Storey, C.L. Liu, P.O. Brown, and D. Herschlag. 2003. Genome-wide analysis of mRNA translation profiles in Saccharomyces cerevisiae. *Proc. Natl. Acad. Sci. USA.* 100:3889–3894. https://doi.org/10.1073/pnas.0635171100

Brandman, O., and R.S. Hegde. 2016. Ribosome-associated protein quality control. *Nat. Struct. Mol. Biol.* 23:7–15. https://doi.org/10.1038/nsmb.3147

Brandman, O., J. Stewart-Ornstein, D. Wong, A. Larson, C.C. Williams, G.W. Li, S. Zhou, D. King, P.S. Shen, J. Weibezahn, et al. 2012. A ribosome-bound quality control complex triggers degradation of nascent peptides and signals translation stress. *Cell.* 151:1042–1054. https://doi.org/10.1016/j.cell.2012.10.044

Brandt, F., S.A. Etchells, J.O. Ortiz, A.H. Elcock, F.U. Hartl, and W. Baumeister. 2009. The native 3D organization of bacterial polysomes. *Cell.* 136:261–271. https://doi.org/10.1016/j.cell.2008.11.016

Brandt, F., L.A. Carlson, F.U. Hartl, W. Baumeister, and K. Grünewald. 2010. The three-dimensional organization of polyribosomes in intact human cells. *Mol. Cell.* 39:560–569. https://doi.org/10.1016/j.molcel.2010.08.003

Buchan, J.R., and R. Parker. 2009. Eukaryotic stress granules: the ins and outs of translation. *Mol. Cell.* 36:932–941. https://doi.org/10.1016/j.molcel.2009.11.020

Buchan, J.R., R.M. Kolaitis, J.P. Taylor, and R. Parker. 2013. Eukaryotic stress granules are cleared by autophagy and Cdc48/VCP function. *Cell.* 153:1461–1474. https://doi.org/10.1016/j.cell.2013.05.037

Chang, H., J. Lim, M. Ha, and V.N. Kim. 2014. TAIL-seq: genome-wide determination of poly(A) tail length and 3′ end modifications. *Mol. Cell.* 53:1044–1052. https://doi.org/10.1016/j.molcel.2014.02.007

Chiabudini, M., A. Tais, Y. Zhang, S. Hayashi, T. Wölfle, E. Fitzke, and S. Rospert. 2014. Release factor eRF3 mediates premature translation termination on polylysine-stalled ribosomes in Saccharomyces cerevisiae. *Mol. Cell. Biol.* 34:4062–4076. https://doi.org/10.1128/MCB.00799-14

Clote, P., Y. Ponty, and J.M. Steyaert. 2012. Expected distance between terminal nucleotides of RNA secondary structures. *J. Math. Biol.* 65:581–599. https://doi.org/10.1007/s00285-011-0467-8

Daneholt, B., K. Anderson, and M. Fagerlind. 1977. Large-sized polysomes in Chironomus tentans salivary glands and their relation to Balbiani ring 75S RNA. *J. Cell Biol.* 73:149–160. https://doi.org/10.1083/jcb.73.1.149

Dewey, C.M., B. Cenik, C.F. Sephton, B.A. Johnson, J. Herz, and G. Yu. 2012. TDP-43 aggregation in neurodegeneration: are stress granules the key? *Brain Res.* 1462:16–25. https://doi.org/10.1016/j.brainres.2012.02.032

Eldad, N., Y. Yosefzon, and Y. Arava. 2008. Identification and characterization of extensive intra-molecular associations between 3′-UTRs and their ORFs. *Nucleic Acids Res.* 36:6728–6738. https://doi.org/10.1093/nar/gkn754

Fang, L.T., W.M. Gelbart, and A. Ben-Shaul. 2011. The size of RNA as an ideal branched polymer. *J. Chem. Phys.* 135:155105. https://doi.org/10.1063/1.3652763

Gaspar, I., F. Wippich, and A. Ephrussi. 2017. Enzymatic production of single-molecule FISH and RNA capture probes. *RNA.* 23:1582–1591. https://doi.org/10.1261/rna.061184.117

Grollman, A.P. 1966. Structural basis for inhibition of protein synthesis by emetine and cycloheximide based on an analogy between ipecac alkaloids and glutarimide antibiotics. *Proc. Natl. Acad. Sci. USA.* 56:1867–1874. https://doi.org/10.1073/pnas.56.6.1867

Harigaya, Y., and R. Parker. 2010. No-go decay: a quality control mechanism for RNA in translation. *Wiley Interdiscip. Rev. RNA.* 1:132–141. https://doi.org/10.1002/wrna.17

Hendrickson, D.G., D.J. Hogan, H.L. McCullough, J.W. Myers, D. Herschlag, J.E. Ferrell, and P.O. Brown. 2009. Concordant regulation of translation and mRNA abundance for hundreds of targets of a human microRNA. *PLoS Biol.* 7:e1000238. https://doi.org/10.1371/journal.pbio.1000238

Hinnebusch, A.G., and J.R. Lorsch. 2012. The mechanism of eukaryotic translation initiation: new insights and challenges. *Cold Spring Harb. Perspect. Biol.* 4:a011544. https://doi.org/10.1101/cshperspect.a011544

Jain, S., J.R. Wheeler, R.W. Walters, A. Agrawal, A. Barsic, and R. Parker. 2016. ATPase-Modulated Stress Granules Contain a Diverse Proteome and Substructure. *Cell.* 164:487–498. https://doi.org/10.1016/j.cell.2015.12.038

Kedersha, N., M.R. Cho, W. Li, P.W. Yacono, S. Chen, N. Gilks, D.E. Golan, and P. Anderson. 2000. Dynamic shuttling of TIA-1 accompanies the recruitment of mRNA to mammalian stress granules. *J. Cell Biol.* 151:1257–1268. https://doi.org/10.1083/jcb.151.6.1257

Kedersha, N., P. Ivanov, and P. Anderson. 2013. Stress granules and cell signaling: more than just a passing phase? *Trends Biochem. Sci.* 38:494–506. https://doi.org/10.1016/j.tibs.2013.07.004

Kedersha, N., M.D. Panas, C.A. Achorn, S. Lyons, S. Tisdale, T. Hickman, M. Thomas, J. Lieberman, G.M. McInerney, P. Ivanov, and P. Anderson. 2016. G3BP-Caprin1-USP10 complexes mediate stress granule condensation and associate with 40S subunits. *J. Cell Biol.* 212:845–860. https://doi.org/10.1083/jcb.201508028

Khong, A., T. Matheny, S. Jain, S.F. Mitchell, J.R. Wheeler, and R. Parker. 2017. The stress granule transcriptome reveals principles of mRNA accumulation in stress granules. *Mol. Cell.* 68:808–820. https://doi.org/10.1016/j.molcel.2017.10.015

Khong, A., S. Jain, T. Matheny, J.R. Wheeler, and R. Parker. 2018. Isolation of mammalian stress granule cores for RNA-Seq analysis. *Methods.* 137:49–54. https://doi.org/10.1016/j.ymeth.2017.11.012

Kim, N.C., E. Tresse, R.M. Kolaitis, A. Molliex, R.E. Thomas, N.H. Alami, B. Wang, A. Joshi, R.B. Smith, G.P. Ritson, et al. 2013. VCP is essential for mitochondrial quality control by PINK1/Parkin and this function is impaired by VCP mutations. *Neuron.* 78:65–80. https://doi.org/10.1016/j.neuron.2013.02.029

Kopeina, G.S., Z.A. Afonina, K.V. Gromova, V.A. Shirokov, V.D. Vasiliev, and A.S. Spirin. 2008. Step-wise formation of eukaryotic double-row polyribosomes and circular translation of polysomal mRNA. *Nucleic Acids Res.* 36:2476–2488. https://doi.org/10.1093/nar/gkm1177

Lai, W.C., M. Kayedkhordeh, E.V. Cornell, E. Farah, S. Bellaousov, R. Rietmeijer, D.H. Mathews, and D.N. Ermolenko. 2018. The formation of intramolec-

ular secondary structure brings mRNA ends in close proximity. bioRxiv. (Preprint posted March 27, 2018). https://doi.org/10.1101/289496

Li, Y.R., O.D. King, J. Shorter, and A.D. Gitler. 2013. Stress granules as crucibles of ALS pathogenesis. *J. Cell Biol.* 201:361–372. https://doi.org/10.1083/jcb.201302044

Mackenzie, I.R., A.M. Nicholson, M. Sarkar, J. Messing, M.D. Purice, C. Pottier, K. Annu, M. Baker, R.B. Perkerson, A. Kurti, et al. 2017. TIA1 mutations in amyotrophic lateral sclerosis and frontotemporal dementia promote phase separation and alter stress granule dynamics. *Neuron.* 95:808–816. https://doi.org/10.1016/j.neuron.2017.07.025

Madin, K., T. Sawasaki, N. Kamura, K. Takai, T. Ogasawara, K. Yazaki, T. Takei, K. Miura, and Y. Endo. 2004. Formation of circular polyribosomes in wheat germ cell-free protein synthesis system. *FEBS Lett.* 562:155–159. https://doi.org/10.1016/S0014-5793(04)00221-2

Milo, R., P. Jorgensen, U. Moran, G. Weber, and M. Springer. 2010. BioNumbers—the database of key numbers in molecular and cell biology. *Nucleic Acids Res.* 38:D750–D753. https://doi.org/10.1093/nar/gkp889

Moon, S.L., T. Morisaki, A. Khong, K. Lyon, R. Parker, and T.J. Stasevich. 2018. Imaging of single mRNA translation repression reveals diverse interactions with mRNP granules. bioRxiv. (Preprint posted May 28, 2018). https://doi.org/10.1101/332692

Morisaki, T., K. Lyon, K.F. DeLuca, J.G. DeLuca, B.P. English, Z. Zhang, L.D. Lavis, J.B. Grimm, S. Viswanathan, L.L. Looger, et al. 2016. Real-time quantification of single RNA translation dynamics in living cells. *Science.* 352:1425–1429. https://doi.org/10.1126/science.aaf0899

Myasnikov, A.G., Z.A. Afonina, J.F. Ménétret, V.A. Shirokov, A.S. Spirin, and B.P. Klaholz. 2014. The molecular structure of the left-handed supra-molecular helix of eukaryotic polyribosomes. *Nat. Commun.* 5:5294. https://doi.org/10.1038/ncomms6294

Namkoong, S., A. Ho, Y.M. Woo, H. Kwak, and J.H. Lee. 2018. Systematic characterization of stress-induced RNA granulation. *Mol. Cell.* 70:175–187. https://doi.org/10.1016/j.molcel.2018.02.025

Palade, G.E. 1955. A small particulate component of the cytoplasm. *J. Biophys. Biochem. Cytol.* 1:59–68. https://doi.org/10.1083/jcb.1.1.59

Panas, M.D., P. Ivanov, and P. Anderson. 2016. Mechanistic insights into mammalian stress granule dynamics. *J. Cell Biol.* 215:313–323. https://doi.org/10.1083/jcb.201609081

Pestka, S. 1971. Inhibitors of ribosome functions. *Annu. Rev. Microbiol.* 25:487–562. https://doi.org/10.1146/annurev.mi.25.100171.002415

Pichon, X., A. Bastide, A. Safieddine, R. Chouaib, A. Samacoits, E. Basyuk, M. Peter, F. Mueller, and E. Bertrand. 2016. Visualization of single endogenous polysomes reveals the dynamics of translation in live human cells. *J. Cell Biol.* 214:769–781. https://doi.org/10.1083/jcb.201605024

Protter, D.S.W., and R. Parker. 2016. Principles and Properties of Stress Granules. *Trends Cell Biol.* 26:668–679. https://doi.org/10.1016/j.tcb.2016.05.004

Ramaswami, M., J.P. Taylor, and R. Parker. 2013. Altered ribostasis: RNA-protein granules in degenerative disorders. *Cell.* 154:727–736. https://doi.org/10.1016/j.cell.2013.07.038

Shoemaker, C.J., and R. Green. 2012. Translation drives mRNA quality control. *Nat. Struct. Mol. Biol.* 19:594–601. https://doi.org/10.1038/nsmb.2301

Shoemaker, C.J., D.E. Eyler, and R. Green. 2010. Dom34:Hbs1 promotes subunit dissociation and peptidyl-tRNA drop-off to initiate no-go decay. *Science.* 330:369–372. https://doi.org/10.1126/science.1192430

Steitz, J.A. 1969. Polypeptide chain initiation: nucleotide sequences of the three ribosomal binding sites in bacteriophage R17 RNA. *Nature.* 224:957–964. https://doi.org/10.1038/224957a0

Van Treeck, B., D.S.W. Protter, T. Matheny, A. Khong, C.D. Link, and R. Parker. 2018. RNA self-assembly contributes to stress granule formation and defining the stress granule transcriptome. *Proc. Natl. Acad. Sci. USA.* 115:2734–2739. https://doi.org/10.1073/pnas.1800038115

Viero, G., L. Lunelli, A. Passerini, P. Bianchini, R.J. Gilbert, P. Bernabò, T. Tebaldi, A. Diaspro, C. Pederzolli, and A. Quattrone. 2015. Three distinct ribosome assemblies modulated by translation are the building blocks of polysomes. *J. Cell Biol.* 208:581–596. https://doi.org/10.1083/jcb.201406040

Wang, C., B. Han, R. Zhou, and X. Zhuang. 2016. Real-Time Imaging of Translation on Single mRNA Transcripts in Live Cells. *Cell.* 165:990–1001. https://doi.org/10.1016/j.cell.2016.04.040

Warner, J.R., A. Rich, and C.E. Hall. 1962. Electron Microscope Studies of Ribosomal Clusters Synthesizing Hemoglobin. *Science.* 138:1399–1403. https://doi.org/10.1126/science.138.3548.1399

Wettstein, F.O., T. Staehelin, and H. Noll. 1963. Ribosomal aggregate engaged in protein synthesis: characterization of the ergosome. *Nature.* 197:430–435. https://doi.org/10.1038/197430a0

Wheeler, J.R., T. Matheny, S. Jain, R. Abrisch, and R. Parker. 2016. Distinct stages in stress granule assembly and disassembly. *eLife.* 5:e18413. https://doi.org/10.7554/eLife.18413

Wolin, S.L., and P. Walter. 1988. Ribosome pausing and stacking during translation of a eukaryotic mRNA. *EMBO J.* 7:3559–3569. https://doi.org/10.1002/j.1460-2075.1988.tb03233.x

Wu, B., C. Eliscovich, Y.J. Yoon, and R.H. Singer. 2016. Translation dynamics of single mRNAs in live cells and neurons. *Science.* 352:1430–1435. https://doi.org/10.1126/science.aaf1084

Yan, X., T.A. Hoek, R.D. Vale, and M.E. Tanenbaum. 2016. Dynamics of Translation of Single mRNA Molecules In Vivo. *Cell.* 165:976–989. https://doi.org/10.1016/j.cell.2016.04.034

Yazaki, K., T. Yoshida, M. Wakiyama, and K. Miura. 2000. Polysomes of eukaryotic cells observed by electron microscopy. *J. Electron Microsc. (Tokyo).* 49:663–668. https://doi.org/10.1093/oxfordjournals.jmicro.a023856

Yoffe, A.M., P. Prinsen, W.M. Gelbart, and A. Ben-Shaul. 2011. The ends of a large RNA molecule are necessarily close. *Nucleic Acids Res.* 39:292–299. https://doi.org/10.1093/nar/gkq642